Korean J. Chem. Eng., **31**(5), 812-820 (2014)
DOI: 10.1007/s11814-014-0006-6

pISSN: 0256-1115
eISSN: 1975-7220

Enhanced Zn(II) uptake using zinc imprinted form of novel nanobiosorbent and its application as an antimicrobial agent

Geetanjali Basak, Devlina Das, and Nilanjana Das†

School of Bio Sciences and Technology, Environmental Biotechnology Division,
VIT University, Vellore-632 014, Tamil Nadu, India
(*Received 12 August 2013 • accepted 6 January 2014*)

Abstract−We investigated the use of zinc imprinted of novel nanobiosorbent prepared from *Candida rugosa* to remove Zn(II) from aqueous solution. The nanobiosorbent was characterized by SEM, FTIR and XRD. Effects of various parameters including pH of the solution, adsorbent dosage, initial Zn(II) ion concentration and contact time on Zn(II) removal by the nanobiosorbents were investigated through batch process. Equilibrium data for Zn(II) removal was fitted to Langmuir isotherm model with an enhanced adsorption capacity of 275.48 mg/g for zinc imprinted *C. rugosa* nanobiosorbent, compared to nonimprinted nanobiosorbent of 172.41 mg/g. Pseudo-second-order kinetic model was best fitted to predict the sorption kinetics for both the nanobiosorbents. AFM study revealed monolayer adsorption with thin film diffusion for Zn(II) removal. The antimicrobial activity of zinc imprinted nanobiosorbent was investigated against pathogenic yeasts *viz. Candida albicans* and *Cryptococcus neoformans* using agar well diffusion method.

Keywords: Adsorption Isotherm Models, *Candida rugosa*, Nanobiosorbent, Non Imprinted, Zinc Imprinted

INTRODUCTION

Over the past few years, nanotechnology has become one of the most popular technologies for the removal of metal cations from aqueous solution. Nanoparticles mainly including nanosized inorganic material derived from metals and metal oxides (i.e., silver nanoparticles, TiO_2, SiO_2, Al_2O_3 and ZnO, Fe_3O_4 [1], magnetic nanoparticles [2], carbon nanotube and synthetic nanoparticles (i.e., synthetic nanostructured Fe(III)-Cr(III) mixed oxide [3] have been applied widely as adsorbents for the treatment of metal cations containing wastewaters. Nanosorbents have been extensively used as they show very attractive properties compared to their bulk form, such as high adsorption capacity, enhanced catalytic activity, high dispersion degree and superparamagnetism behavior [4,5] due to various advantages such as (i) tiny particulate diameter, (ii) large external surface area, (iii) high density of reactive surface sites, and (iv) great intrinsic reactivity of surface sites and small internal diffusion resistance [6] These chemically synthesized nanosorbents have several disadvantages, such as high preparation cost, strict operational conditions, and high energy consumption, which might limit the application of nanosorbents for wastewater treatment. Therefore, nanobiosorbents (*Pleurotus ostreatus*) as an alternate to chemical nanosorbent have been applied for the removal of metal cations from wastewater [7]. To date, no work has been reported about the applicability of yeast as nanobiosorbent for the removal of heavy metal cations from industrial wastewater.

Compared to bacteria and filamentous fungi, yeasts are inexpensive and readily available sources of biomass, can grow faster than most filamentous fungi, and have the ability to resist unfavourable conditions. Yeasts can adapt and grow under various extreme conditions of pH, temperature and nutrient availability as well as high pollutant concentration [8].

Recently, research on developing selective adsorption has been directed to the molecular imprinting process. Metal ion imprinting technology is a method developed on molecular imprinting, mainly for making selective binding sites in synthetic polymers y busing a metal ion template. After the removal of the template, the remaining polymer is more selective [9,10]. It includes the copolymerization of functional and cross-linking monomers in the presence of the target analyte, the imprint molecule [11]. The surface imprinted adsorbent combines the advantages of good adsorption ability and stability [12]. Therefore, it is an effective and powerful method for the removal of metal ions. Thus, the binding of chitosan onto dead biomass of *C. rugosa* nanobiosorbent by metal ion imprinting technology will probably yield another novel metal imprinted *C. rugosa* nanobiosorbent for the effective removal of heavy metal ions, owing to the high selectivity for the target ions and quick separation from aqueous solution.

Zinc has increasingly been used in various industries: sheet metal galvanization, manufacture of alloys, TV picture tubes, etc. This has resulted in the discharge of industrial effluents into natural water systems adjoining landmasses and sewer systems from small and medium scale industries. This poses serious problems to the environment and ecosystems. In the Dangerous Substances Directive (76/464/EEC) of the European Union, zinc has been registered as List 2 Dangerous substance with Environmental Quality Standards being set as 40 μg/L for estuaries and marine waters and at 45-500 μg/L for freshwater depending on water hardness [13]. According to the WHO more than 3 mg/L of Zn(II) in drinking water is unacceptable. In addition, too much intake of Zn(II) can increase respiratory activities such as breathing rate, volume and frequency of ventilation, coughing, decrease in oxygen uptake efficiency [14].

†To whom correspondence should be addressed.
E-mail: nilanjana00@lycos.com

To the best of our knowledge, no report is available on the application of zinc imprinted and nonimprinted nanobiosorbent for the removal of Zn(II) ions from aqueous solution. Therefore, the main objective of the present study was to compare the potential of zinc imprinted and nonimprinted nanobiosorbent *C. rugosa* in the removal of the Zn(II) from aqueous solutions. The adsorption of Zn(II) ions onto zinc imprinted and nonimprinted *C. rugosa* nanobiosorbent was studied in batch experiments. Adsorption isotherms and kinetics models were conducted to describe the experimental data and understand the adsorption mechanism. In addition, the antimicrobial activity of zinc imprinted and nonimprinted *C. rugosa* nanobiosorbent against pathogenic yeast species *viz. C. albicans* and *C. neoformans* was studied.

EXPERIMENTAL

1. Metal Solution Preparation

Zn(II) stock solution was prepared (1,000 mg/L) by dissolving 4.55 g of powdered $Zn(NO_3)_2 \cdot 6H_2O$ (Hi Media, Mumbai, India) in 1,000 mL of deionized water. The working solutions of metal were prepared by diluting the stock solution to the desired concentrations.

2. Microorganism and Preparation of Non Imprinted Nanobiosorbent

Effluent sample was collected from Common Effluent Treatment Plant (CETP), Ranipet, Vellore, Tamilnadu, India. Sample was serially diluted from 10^{-1} to 10^{-6} fold and was plated on yeast extract peptone dextrose (YEPD) media by spread plate technique. Morphologically distinct colonies were isolated and subcultured on YEPD agar. It was phenotypically characterized and identified to a species level as *C. rugosa* by VITEK 2 Compact Yeast card reader with software version V2C 03.01 at the Council for Food Research and Development (CFRD), Kerala, India. The isolate was maintained in yeast extract peptone dextrose (YEPD) agar slants at 4 °C. Mass cultivation of yeast isolate was carried out in inexpensive sugarcane bagasse extract medium as reported in our previous study [15]. The yeast biomass was harvested by centrifugation at 10,000 rpm for 5 min and dried in oven at 60 °C. Then the dried *C. rugosa* was ground into powder with a pulverizing mill (Pulverisette 7 monomill, Fristch) to obtain raw biomass for further use.

The possible functional groups present in the nonimprinted nanobiosorbent used in this study were characterized with Fourier transform infrared spectrometer (Shimadzu IR affinity-1). The nanobiosorbent was further characterized by SEM scanning electron microscopy (Hitachi-S-3400). The size distribution of nonimprinted nanobiosorbent was measured by X-ray diffraction (XRD) (D8 Advance: Bruker, Germany).

3. Preparation of Zinc Imprinted *C. rugosa* Nanobiosorbent

The zinc imprinted *C. rugosa* nanobiosorbent was prepared following the standard methodology [11]. $Zn(NO_3)_2 \cdot 6H_2O$ was dissolved in 2 cm^3 dilute acetic acid solution (2.5% v/v) to give a Zn^{2+} solution of 2 mg/cm^3. Then 0.1 g chitosan (dry weight) was dissolved in this solution. Two grams of native *C. rugosa* nanobiosorbent (nonimprinted) and deionized water were added to the above solution and the mixture was stirred. Then, 0.5 cm^3 epichlorohydrin as cross-linking agent was added into the mixture and allowed to carry out for 4-6 h at room temperature. The product was recovered by treating the mixture with EDTA solution containing 0.2 g/L for 8-12 h. The surface imprinted nanobiosorbent was filtered by using filter paper and dried at 60 °C for 12 h.

4. Batch Adsorption Studies

To study the effect of parameters, all the experiments were performed separately containing zinc imprinted and nonimprinted nanobiosorbents along with 50 mL of solution in each flask at 30 °C with a shaking speed of 120 rpm. The effect of pH (2.0-10.0), sorbent dosage (0.08-1.0 g/L), initial metal concentration (10-100 mg/L) and contact time (30-300 min) on removal of zinc was investigated. The experiments were optimized at the desired pH, metal concentration, sorbent dosage and contact time using 100 mL of Zn(II) test solution in 250 mL Erlenmeyer flask. After adsorption, the suspension was centrifuged for 5 min at the shaking speed of 10,000 rpm. The residual supernatants were determined by Atomic absorption spectrophotometer (Varian AA-240, Australia). The Zn(II) adsorption capacity (q_e) was calculated as follows:

$$q_e = \frac{C_0 - C_e}{m} \times V \quad (1)$$

where C_e (mg/L) is the equilibrium concentration of Zn(II) ion, V (L) is the volume of the solution and m (g) is the mass of the adsorbent.

The Zn(II) removal percentage was calculated with the following equation:

$$\text{Zn(II) removal } \% = \frac{C_0 - C_f}{C_0} \times 100 \quad (2)$$

where C_0 is the initial Zn(II) concentration (mg/L) and C_f is the final Zn(II) concentration (mg/L).

5. Equilibrium and Kinetic Studies

The experimental equilibrium data were analyzed by Langmuir [16], Freundlich [17] and Dubinin-Radushkevich (D-R) [18] isotherms, respectively, to assess the mode of adsorption. The kinetic constants were evaluated by using pseudo-first-order [19] and pseudo-second-order [20] kinetic models. The nature of Zn(II) adsorption was determined using intraparticle diffusion and Boyd plot [21]. A mass transfer plot [22] was used to determine the mass transfer coefficient values for the removal of Zn(II) by zinc imprinted and nonimprinted *C. rugosa* nanobiosorbent, respectively.

6. Atomic Force Microscopic Studies

Atomic force microscopy (Nanosurf easyscan 2, Switzerland) was used to observe the surface morphology of zinc imprinted and nonimprinted nanobiosorbents before and after interaction with Zn(II) ions.

7. Agar Well Diffusion Method for Antimicrobial Activity

Two pathogenic yeast isolates, *Candida albicans* and *Cryptococcus neoformans*, were collected from CMC, Department of Microbiology, Bagayam, Thorapadi, Vellore, Tamil Nadu, India. Antimicrobial assay of the nonimprinted and zinc imprinted *C. rugosa* nanobiosorbent was determined by agar well diffusion assay. Approximately 20 mL of sterile molten and cooled media Mueller Hinton Agar (MHA) was poured in sterilized petri plates and kept at room temperature overnight to check for any contamination to appear. The target yeasts were inoculated and wells were prepared using a sterilized stainless steel cork borer of diameter 5 mm. Each plate containing four wells was filled with distilled water, tetracycline, nonimprinted and zinc imprinted nanobiosorbent. The plates were incubated at

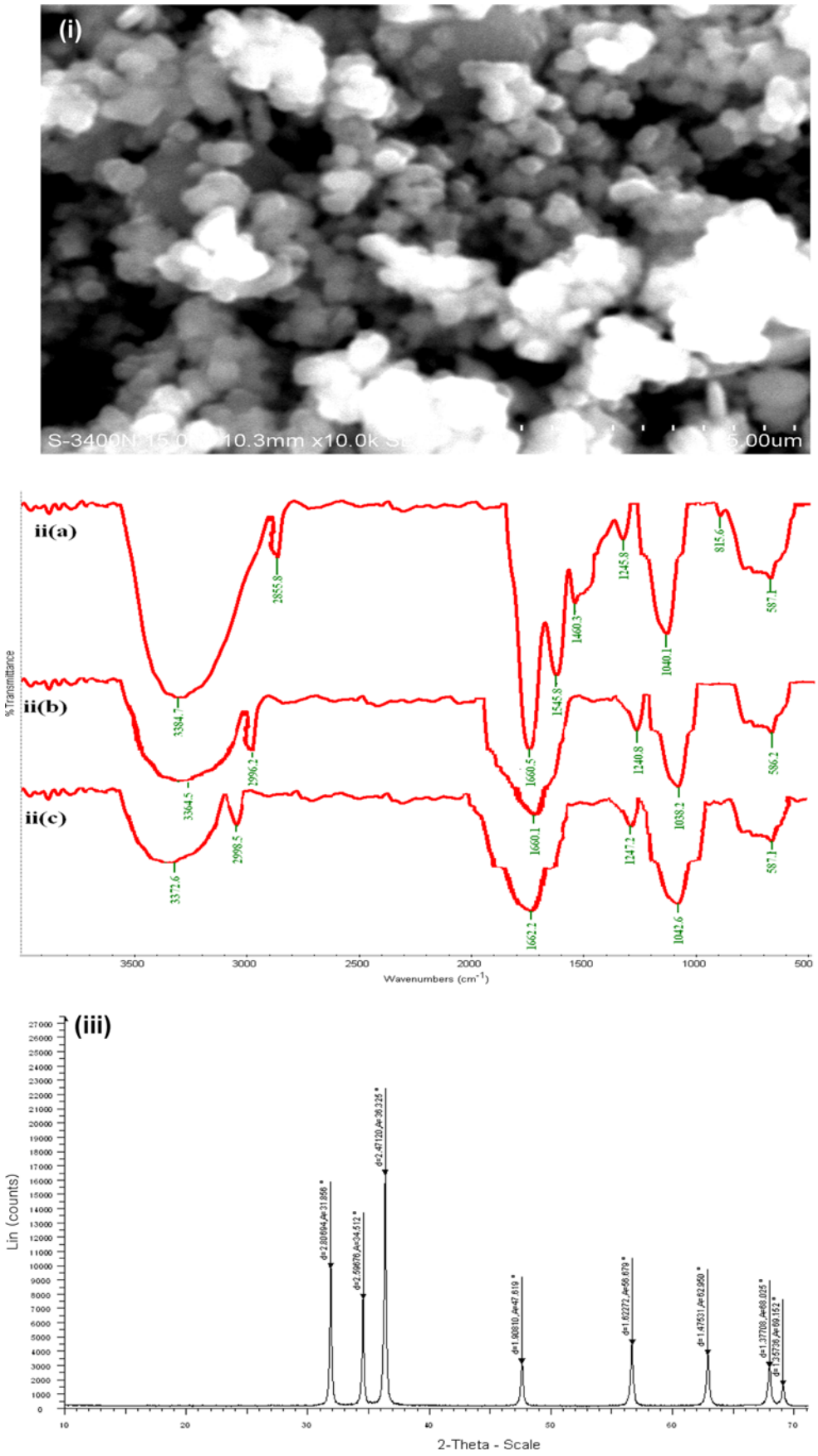

Fig. 1. Characterization of nonimprinted *C. rugosa* nanobiosorbent by (i) SEM (ii) FTIR (a) non imprinted *C. rugosa* nanobiosorbent, (b) native zinc imprinted *C. rugosa* nanobiosorbent, (c) Zn(II) interacted zinc imprinted *C. rugosa* nanobiosorbent, and (iii) XRD.

37 °C for 24 h and the zone of inhibition was calculated by deducing the well diameter from the total inhibition zone diameter [23].

RESULTS AND DISCUSSION

1. Characterization of Nanobiosorbent

1-1. Scanning Electron Microscope (SEM)

SEM micrograph of nonimprinted *C. rugosa* nanobiosorbent, showed that the surface of nonimprinted *C. rugosa* nanobiosorbent was rough with many tiny interspaces structure so that metal in the solution can be adsorbed easily by the adsorbents (Fig. 1(i)). This could be attributed to the considerable loss of moisture from the cell wall, thereby resulting in the shrinkage of the cells.

1-2. Fourier Transform Infrared Spectrum (FTIR)

FTIR spectrum of the nonimprinted *C. rugosa* nanobiosorbent is shown in Fig. 1(iia). The peaks obtained at 3,384.7, 2,855.8, 1,660.5, 1,245.8 and 1,040.1 cm^{-1} indicated the O-H and N-H stretching vibration, strong CH antisym and sym stretching of (methyl) CH_3 group, C=O stretching, C-O-C antisym stretch in esters and lactones and C-N stretching vibrations of aliphatic and aromatic amines, respectively [7,24]. These functional groups might play an important role in the process of Zn(II) removal. In case of zinc imprinted *C. rugosa* nanobiosorbent, the peaks noted at 3,364.5, 2,996.2, 1,660.1, 1,240.8 and 1,038.2 indicated the presence of O-H and N-H stretching vibration, strong CH antisym and sym stretching of (methyl) CH_3 group, C=O stretching, C-O-C antisym stretch in esters and lactones and C-N stretching vibrations of aliphatic and aromatic amines, respectively (Fig. 1(iib)). These peaks were shifted to 3,372.6, 1,662.2, 1,247.2 and 1,042.6, respectively, for Zn(II) interacted zinc imprinted *C. rugosa* nanobiosorbent (Fig. 1(iic)), indicating hydroxyl, amine and carbonyl groups were responsible for Zn(II) removal. Zn(II) ions will form complexes with these functional groups and will be removed from the aqueous solution.

1-3. X-ray Diffraction (XRD)

The structural facets of nonimprinted *C. rugosa* nanobiosorbent were elucidated by the XRD spectrum (Fig. 1(iii)). The peaks at 2θ values of 31.85°, 34.51°, 36.32°, 47.61°, 56.67°, 62.95°, 68.02° and 69.15° corresponded to the crystal planes of (100), (002), (101), (102), (110) and (103), (112) and (201) hexagonal wurtzite phase of nanobiosorbent. The diameter of nanobiosorbent was calculated using the Debye-Scherrer formula [25].

$$d = \frac{0.89\lambda}{\beta\cos\theta} \tag{3}$$

where 0.89 is Scherrer's constant, λ is the wavelength of X-rays, θ is the Bragg diffraction angle and β is the full width at half-maximum (FWHM) of the diffraction peak corresponding to plane (101). The average particle size of the nanobiosorbent was determined from the FWHM of more intense peak corresponding to 101 plane located at 36.32° and was found to be 5.01 nm.

2. Batch Adsorption Experiments

2-1. Effect of pH

The effect of pH on removal of Zn(II) ions by zinc imprinted and nonimprinted *C. rugosa* nanobiosorbent was evaluated in the range

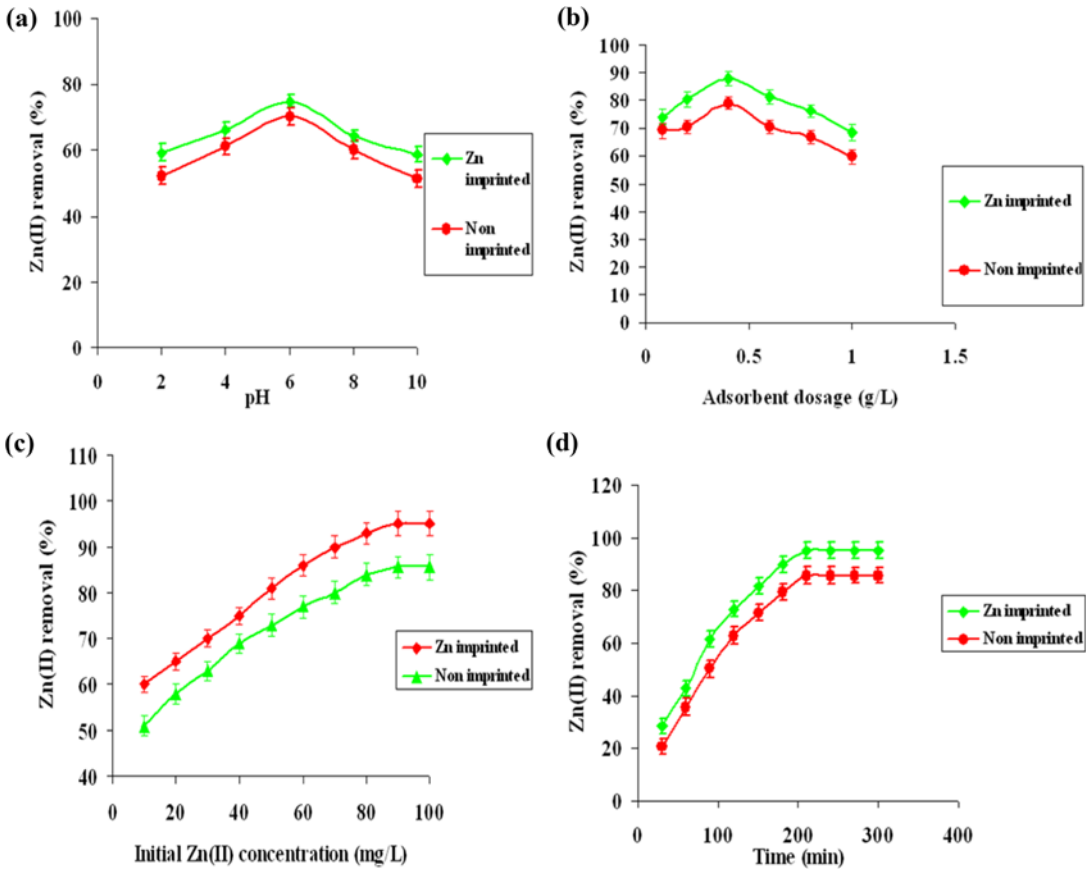

Fig. 2. Effect of operational parameter on Zn(II) removal (a) pH, (b) adsorbent dosage, (c) initial Zn(II) concentration, (d) contact time.

of 2-10 (Fig. 2(a)). Maximum Zn(II) removal in case of both type of nanobiosorbents was noted at a pH of 6. This could be possibly due to the decrease in number of protons that led to a decrease in the competition between proton and metal cations. Ion exchange played the key role in the increasing of Zn(II) removal when pH increased [7]. Maximum Zn(II) removal was noted by zinc imprinted *C. rugosa* nanobiosorbent (75.0%) followed by nonimprinted *C. rugosa* nanobiosorbent (70.2%).

2-2. Effect of Adsorbent Dosage

The adsorbent dosage is one of the important parameters in Zn(II) removal studies because it determines the capacity of adsorbent for a given initial concentration of Zn(II) solution. Fig. 2(b) shows the effect of adsorbent dosage on Zn(II) removal at a range of 0.04-1.0 g/L. Zn(II) removal percentage was found to increase with an increase in the adsorbent dosage upto 0.4 g/L. Owing to the presence of the maximum number of protonated amine groups and exchangeable ions, zinc imprinted *C. rugosa* nanobiosorbent was found to exhibit maximum Zn(II) removal percentage of 88.01%, followed by nonimprinted *C. rugosa* nanobiosorbent (79.03%). A decrease in Zn(II) removal percentage was noted with an increase in nanosorbent dosage beyond 0.4 g/L. This could probably be due to the overlapping of nanosorbent particles that blocked the combination of Zn(II) ions with active sites of nanobiosorbents [7].

2-3. Effect of Initial Zn(II) Ion Concentration

The effect of initial Zn(II) concentration on removal of Zn(II) ion onto nonimprinted and zinc imprinted *C. rugosa* nanobiosorbents was investigated in the concentration ranging from 10-100 mg/L (Fig. 2(c)). An increase in Zn(II) concentration upto 90 mg/L was found to enhance the Zn(II) removal percentage in case of both the nanobiosorbents, which was due to the sufficient availability of Zn(II) ions that provided a driving force to overcome mass transfer resistance [26]. Hence, it could be inferred that the optimum initial Zn(II) concentration in the present study was 90 mg/L.

2-4. Effect of Contact Time

The removal of Zn(II) ions by nonimprinted and zinc imprinted *C. rugosa* nanobiosorbent was studied as a function of contact time ranging from 30 to 300 mins (Fig. 2(d)). The Zn(II) removal efficiency for both the nanobiosorbents reached equilibrium at 210 min. In the initial stages, the metal removal efficiencies of nanobiosorbents increased rapidly due to abundant availability of active binding sites on the nanobiosorbents, and with gradual occupancy of these sites the sorption became less efficient in the later stages [26].

Under optimum conditions, that is, pH 2, adsorbent dosage 0.4 g/L, temperature 30 °C, contact time 210 min and initial Zn(II) concentration of 90 mg/L, maximum Zn(II) removal 95.12% was noted in case of zinc imprinted *C. rugosa* nanobiosorbent followed by 85.6% of nonimprinted nanobiosorbent, respectively.

3. Adsorption Isotherms

The sorption isotherm is the relationship between equilibrium concentration of metal ions in the liquid phase and equilibrium concentration of metal ions in the nanosorbent at constant temperature during the adsorption process, and it can be expressed by various isotherm models. We used three common and important isotherm equations, Langmuir, Freundlich and D-R, to evaluate the adsorption process.

3-1. Langmuir Adsorption Isotherm

The Langmuir isotherm assumes monolayer mode of adsorption. There would be no migration of adsorbed ion at the sites of adsorbate when the process reached equilibrium [14]. The equation is expressed as follows:

$$q_{eq} = \frac{q_{max} K_L C_{eq}}{1 + K_L C_{eq}} \tag{4}$$

which can be linearized as:

$$\frac{1}{q_{eq}} = \frac{1}{q_{max}} + \frac{1}{K_L q_{max} C_{eq}} \tag{5}$$

where q_{eq} (mg/g) is the Zn(II) uptake at equilibrium, C_{eq} (mg/L) is the residual concentration in the supernatant, q_{max} (mg/g) is the maximum Zn(II) uptake value and K_L (L/g) is the adsorption constant related to the free energy of biosorption.

A plot of $1/q_e$ vs $1/C_e$ was obtained to calculate the Langmuir coefficients as shown in Fig. 3(a). The data was found to appropriately fit in the Langmuir isotherm with regression values of 0.9732 and 0.9722 in case of zinc imprinted and nonimprinted *C. rugosa* nanobiosorbent, respectively.

3-2. Freundlich Adsorption Isotherm

The Freundlich equation based on sorption on a heterogeneous surface is given below as Eq. (7):

$$q_e = K_F C_e^{1/n} \tag{6}$$

where K_F and n are Freundlich constants, whereas K_F and n are indicators of adsorption capacity and adsorption intensity of the sorbents, respectively [17]. Eq. (6) can be linearized in logarithmic form as Eq. (7)

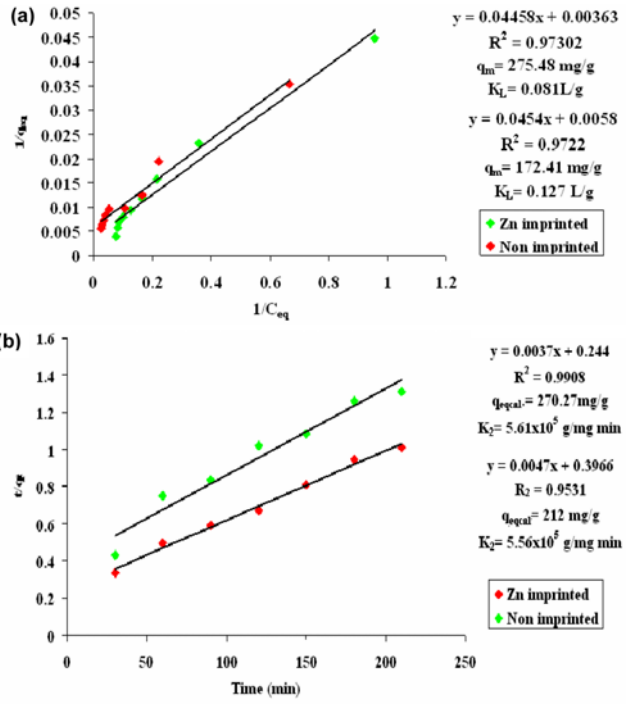

Fig. 3. (a) Langmuir isotherm of Zn(II) adsorption onto zinc imprinted and nonimprinted *C. rugosa* nanobiosorbent at different Zn(II) concentrations. (b) Pseudo-second-order kinetics of Zn(II) adsorption onto zinc imprinted and nonimprinted *C. rugosa* nanobiosorbent at different Zn(II) concentrations.

Table 1. Isotherm constants and kinetic models for Zn(II) removal by zinc imprinted and non imprinted *C. rugosa* nanobiosorbent

Isotherm constant	Zinc imprinted	Non imprinted
Langmuir		
Equation	y=0.0445x+0.0036	y=0.0454x+0.0058
q_m (mg/g)	275.48	172.41
K_L (L/g)	0.081	0.127
R^2	0.9730	0.9722
Freundlich		
Equation	y=0.8771x+1.2723	y=0.5263x+1.4504
K_F (L/g)	18.71	28.18
n	1.14	1.90
R^2	0.9536	0.9450
D-R		
Equation	y=−1.462x+5.3178	y=−1.3848x+5.3178
q_m (mg/g)	207.8	90.99
B (mol^2/J^2)	0.731	0.722
E (KJ/mol^2)	1.1696	1.1768
R^2	0.8741	0.8650
Kinetic constants		
Pseudo-first order		
Equation	y=−0.0028x+2.2873	y=−0.0038x+2.2113
K_{ip} (1/min)	0.0064	0.0087
R^2	0.9693	0.9341
Pseudo-second order		
Equation	y=0.0037x+0.244	y=0.0047x+0.3966
K_2 (g/mg min)	5.61×10^5	5.56×10^5
R^2	0.9908	0.9531
Intraparticle diffusion		
Equation	y=12.989x+23.913	y=9.764x+9.7352
K_p (mg/g min)	12.989	9.764
R^2	0.967	0.937
Mass transfer Kinetics		
Equation	y=−0.0023x+2.6486	y=−0.0067x+0.7732
K_a (L/g)	22.31	21.89
S_s (m^2/g)	29.2	25.6
B_L (m/s)	0.00007	0.0002
R^2	0.9462	0.9268

$$\log q_{eq} = \log K_F + \frac{1}{n}\log C_{eq} \tag{7}$$

The values of Freundlich constants were calculated from the intercepts and slope of the plot (Table 1). The R^2 values were 0.9536 and 0.9450 for zinc imprinted and nonimprinted *C. rugosa* nanobiosorbent, respectively. However the values R^2 were lower than for the Langmuir isotherm. A value for n above one indicates a normal Langmuir isotherm, while n below one is indicative of cooperative adsorption [27,28].

3-3. Dubinin-Radushkevich Isotherm

This isotherm is generally expressed as follows [29]:

$$\ln q_e = \ln q_D - 2B_D[RT \ln(1+1/C_e)) \tag{8}$$

Here the characteristic sorption curve is related to the porous structure of the sorbent. The constant, B_D, is related to the mean free energy of sorption per mole of the sorbate as it is transferred to the surface of the solid from infinite distance in the solution, and this energy can be computed using the following relationship [30]:

$$E = \frac{1}{\sqrt{2B_D}} \tag{9}$$

The linear Dubinin-Radushkevich isotherm plots for the removal of the Zn(II) ions onto zinc imprinted and nonimprinted *C. rugosa* nanobiosorbent are presented in Table 1, and the result showed that the experimental data do not correlate with the Dubinin-Radushkevich equation. This was confirmed by the R^2 values (0.8741 and 0.8650) for zinc imprinted and nonimprinted *C. rugosa* nanobiosorbent, respectively.

4. Kinetic Studies

To evaluate the adsorption kinetic mechanism that controls the adsorption process, five kinetic models including pseudo-first-order, pseudo-second-order, intra-particle diffusion , mass transfer and Boyd plot model were used.

Kinetic parameters from linear plots of four kinetic models are given in Table 1.

The pseudo-first-order rate expression of the Lagergren model is generally expressed as follows:

$$\log(q_{eq} - q_t) = \log q_e - \frac{K_1}{2.303}t \tag{10}$$

where K_{ip} (1/min), is the rate constant, q_e (mg/g) is the amount of solute adsorbed on the surface at equilibrium and q_t (mg/g) is the amount of solute adsorbed at any time. From the plot log ($q_e - q_t$) against t, values of K_{ip} for both the nanobiosorbents were calculated. The first-order equation of Lagergren for both the zinc imprinted and nonimprinted *C. rugosa* nanobiosorbent does not fit well to the whole range of contact time and is generally applicable over the initial stage of the adsorption processes (Fig. 4(a)). The results demonstrated that there was no significant relationship between the kinetic data (figures not shown) with low correlation coefficients (>0.97), indicating that this model is not applicable in the present case. Therefore, the pseudo-second-order kinetic model [31] as shown in Eq. (10) was used to study the kinetics of the present system. Fig. 3(b) represents the pseudo-second-order kinetic model for both the nanobiosorbents.

$$\frac{t}{q_t} = \frac{1}{K_2 q_{eq}^2} + \left(\frac{1}{q_{eq}}\right)t \tag{11}$$

where K_2 (g/mg min) is the second-order rate constant. From the slope and intercepts of the plot t/q_t versus t, q_{eq} and K_2 were calculated. The initial sorption rate h (mg/g min) for both the yeast species was calculated from the second-order rate constant K_2, where t tends to 0.

$$h = K_2 q_{eq}^2 \tag{12}$$

The pseudo-second-order model showed the best fit among all the models in case of both the nanobiosorbents R^2. High correlation coefficients of 0.9908 and 0.9531 in case of zinc imprinted and nonimprinted *C. rugosa* nanobiosorbent respectively. This suggested that adsorption process was controlled by chemisorption. The equi-

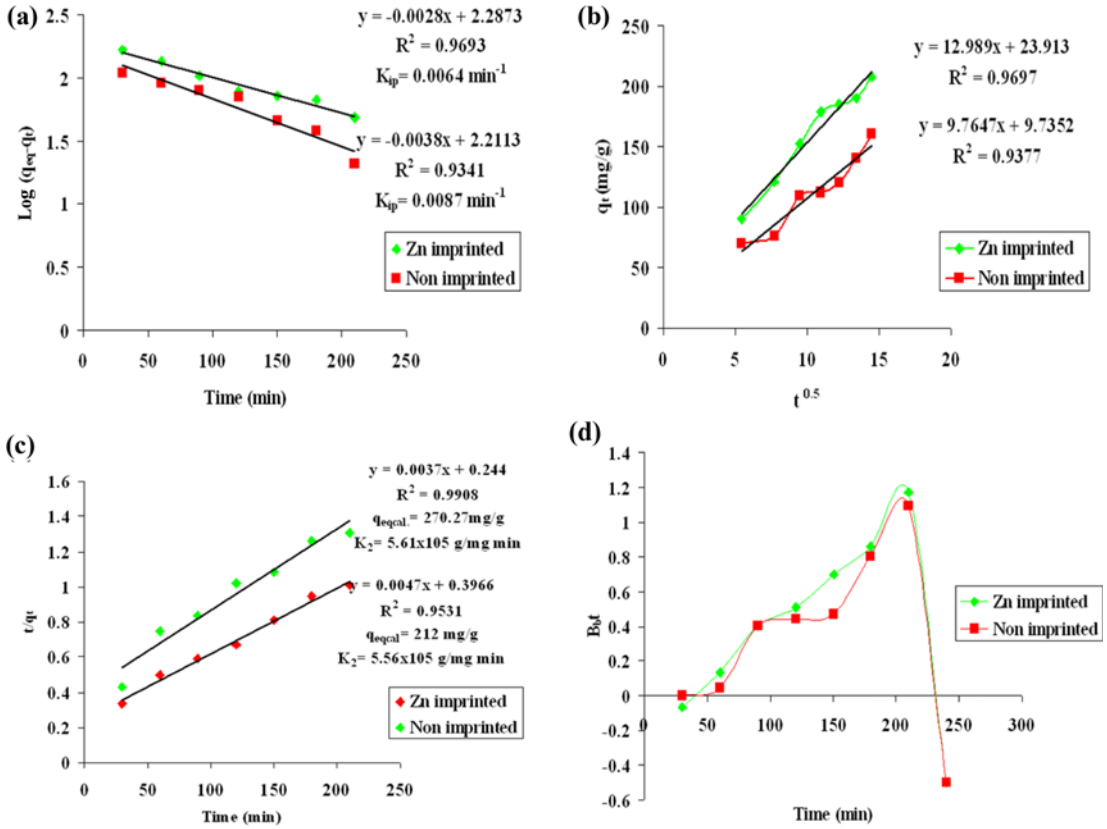

Fig. 4. Kinetic models (a) pseudo-first-order, (b) intraparticle diffusion, (c) boyd plot, (d) mass transfer for Zn(II) adsorption onto zinc imprinted and nonimprinted *C. rugosa* nanobiosorbent at different Zn(II) concentrations.

librium uptake, q_e, obtained from this model is closely in line with the experimental value.

The intra-particle diffusion coefficient for the removal of Zn(II) was calculated from the slope of the plot between the amount of Zn(II) sorbed, q_t (mg /g) vs $t^{0.5}(min^{0.5})$. Based on this plot (Fig. 4(b)), we concluded that the removal process of Zn(II) by zinc imprinted and nonimprinted *C. rugosa* nanobiosorbent is comprised of three phases, suggesting that the intraparticle diffusion is not the rate-limiting step for the whole reaction. The uptake rate was initially very fast, then medium finally giving way to slow uptake. It is likely that the adsorbate was initially transported to macro, then meso and finally slowly diffused into micropores [32]. Moreover, low correlation coefficients for intra-particle diffusion model followed by zinc imprinted and nonimprinted *C. rugosa* nanobiosorbent signified the invalidation of the model.

The kinetic data were further analyzed by using the kinetic expression given by Boyd et al. [33] to check whether sorption proceeds via film diffusion or intra-particle diffusion mechanism, which is expressed as follows:

$$F = 1 - \frac{6}{\pi^2}\exp(-B_b t) \tag{13}$$

where B_b is a constant and F is the fractional attainment of equilibrium at time t given by

$$F = \frac{q_t}{q_e} \tag{14}$$

where q_e and q_t represent the amount of Zn(II) ion sorbed (mg/g) at equilibrium and any time t, respectively. To compute $B_b t$, Eq. (13) is substituted into Eq. (14) and the kinetic expression becomes

$$B_b t = -0.4977 - \ln\left(1 - \frac{q_t}{q_e}\right) \tag{15}$$

Linearity of this plot is employed to distinguish between external transport-(film diffusion) and intra-particle transport-controlled rates of sorption [34]. A straight line passing through the origin is indicative of sorption processes governed by particle-diffusion mechanisms; otherwise they are governed by film diffusion [35]. In the present case, the plots were neither linear nor passed through the origin (Fig. 4(c)), which showed that film diffusion was the rate-limiting sorption process for Zn(II) removal onto zinc imprinted and nonimprinted *C. rugosa* nanobiosorbents.

The solute transfer is frequently controlled by resistance to external mass transfer (boundary layer diffusion) in the solid-liquid sorption process [22]. The following equation of the model is expressed as follows:

$$\ln\left(\frac{C_t}{C_0} - \frac{1}{1+mK_a}\right) = \ln\left(\frac{mK_a}{1+mK_a}\right) - \left(\frac{1+mK_a}{mK_a}\right)B_l S_s t \tag{16}$$

where C_t and C_0 (both in mg/L) are the concentrations of sorbent at time t and zero, respectively; K_a (L/g) is a constant defined as the product of the Langmuir constants (q_mK), m (g/L) and S_s (m^2) are the adsorbent mass and surface area, respectively. The coefficient B_L can be calculated from the slope of the regression line: ln[(C_t/

$C_0)-(1/1+mK_a)]$ vs t. The coefficient B_l can be calculated from the slope of the plot $\ln[(C_t/C_0)-(1/1+mK_a)]$ vs. t (the slope coefficient was determined by a linear regression analysis). From the Fig. 4(d), the regression values were maximum in case of zinc imprinted *C. rugosa* nanobiosorbent (0.9462) followed by nonimprinted *C. rugosa* nanobiosorbent (0.9268) for Zn(II) removal. The B_l value was minimum in case of zinc imprinted *C. rugosa* nanobiosorbent (0.00007 m/s) followed by nonimprinted *C. rugosa* nanobiosorbent (0.0002 m/s). This suggested that minimum mass transfer required for the removal of Zn(II) ion onto zinc imprinted *C. rugosa* nanobiosorbent validating the maximum uptake of Zn(II) ion by zinc imprinted *C. rugosa* nanobiosorbent.

5. Atomic Force Microscopy (AFM)

The atomic force microscopic images demonstrated the topological appearance of the nonimprinted *C. rugosa* nanobiosorbent before (Fig. 5(a1)) and after Zn(II) interaction (Fig. 5(a2)) as well as zinc imprinted *C. rugosa* nanobiosorbent before (Fig. 5(b1)) and after Zn(II) interaction (Fig. 5(b2)). The AFM images were used to analyze the adsorption behavior of the nanobiosorbents. AFM image of the nanobiosorbents interacting with Zn(II) ions showed the homogeneous mode of adsorption as a thin film supporting the monolayer adsorption and thin film diffusion as shown by Langmuir isotherm model and Boyd plot model, respectively.

6. Evaluation of Antimicrobial Activity by Agar Well Diffusion Method

Antimicrobial effects of nonimprinted and zinc imprinted nanobiosorbents are shown in Fig. 6 as indicated by zone of inhibition, respectively, for pathogenic yeasts: *Candida albicans* (Fig. 6(a)) and *Cryptococcus neoformans* (Fig. 6(b)). The zinc imprinted nanobiosorbents showed a greater effect on *Candida albicans* compared to *Cryptococcus neoformans*. The order of zone of inhibition was as follows: zinc imprinted nanobiosorbent (22.3±0.05/20.2±0.1 mm)> Tetracycline (21.03±0.1/16.4±0.12 mm)>nonimprinted nanobiosorbent (19.1±0.1/10.2±0.3 mm)>control (0.0±0.0/0.0±0.0 mm).

CONCLUSIONS

The results presented in this paper demonstrated the application of zinc imprinted and nonimprinted form of novel nanobiosorbent prepared from *Candida rugosa* for removal of Zn(II) ions from aqueous solution. Zn(II) removal was found to be maximum at an optimum pH 6.0; adsorbent dosage 0.4 g/L; 90 mg/L of initial Zn(II) concentration and 210 min contact time. Equilibrium sorption data showed excellent fit to Langmuir isotherm model, indicating a monolayer mode of Zn(II) adsorption on the surface of zinc imprinted *C. rugosa* nanobiosorbent. The result of adsorption kinetic study of

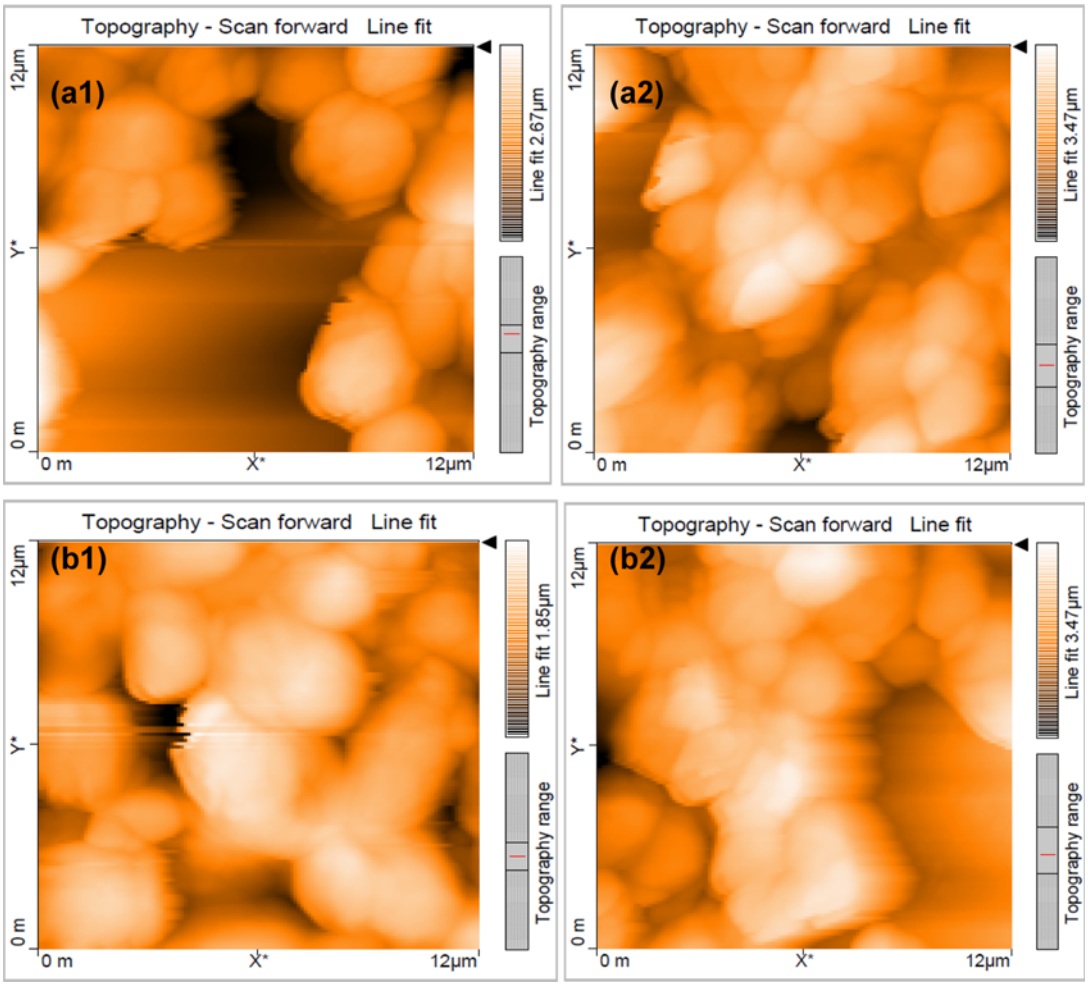

Fig. 5. AFM images of (a) nonimprinted (b) zinc imprinted (1) before and (2) after interaction with Zn(II) ions.

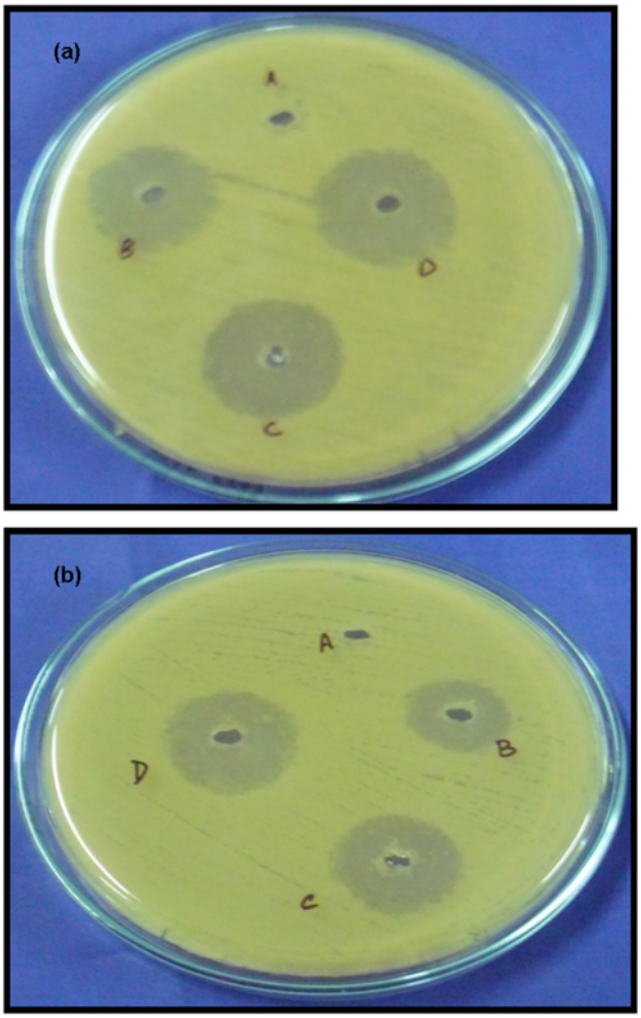

Fig. 6. Zone of inhibition against (a) *C. albicans* and (b) *C. neoformans* at (A) Control (B) Tetracyclin (C) nonimprinted and (D) zinc imprinted *C. rugosa* nanobiosorbent.

Zn(II) on zinc imprinted *C. rugosa* nanobiosorbent indicated that the adsorption kinetics followed the pseudo-second-order model with thin film diffusion as rate-limiting step. Enhanced antimicrobial activity was noted in case of zinc imprinted *C. rugosa* nanobiosorbent, depicting the potentiality of surface imprinting technology during the process of adsorption.

ACKNOWLEDGEMENTS

The authors would like to thank VIT University for providing the laboratory facility and financial support for the smooth conduct of the work. We also extend our gratitude towards Pondicherry University for the assistance in SEM analysis. Also, sincere gratitude to nanotechnology laboratory, VIT University for providing us with AFM facility during the course of our work.

REFERENCES

1. X. S. Wang, H. J. Lu, F. Liu and J. J. Ren, *Adsorpt. Sci. Technol.*, **26**, 407 (2011).
2. L. Giraldo, A. Erto and J. C. Moreno-Pirajañ, *Adsorption*, **19**, 465 (2013).
3. T. Basu and U. C. Ghosh, *Desalination*, **266**, 25 (2011).
4. N. N. Nassar, A. Hassan and P. Pereira-Almao, *Energy Fuels*, **25**, 1566 (2011).
5. N. N. Nassar, A. Hassan and P. Pereira-Almao, *Energy Fuels*, **25**, 1017 (2011).
6. R. Rakhshaee, *J. Hazard. Mater.*, **197**, 144 (2011).
7. L. Ma, Y. Peng, B. W. D. Lei and H. Xu, *Chem. Eng. J.*, **225**, 59 (2013).
8. D.Charumathi and N. Das, *Int. J. Eng. Sci. Technol.*, **2**, 4325 (2010).
9. R. Say, M. Erdem, A. Ersoz, H. Turk and A. Denizli, *Appl. Catal. A.*, **286**, 221 (2005).
10. T. P. Rao, R. Kala and S. Daniel, *Anal. Chim. Acta*, **578**, 105 (2006).
11. Z. C. Li, H. T. Fan, Y. Zhang, M. X. Chen, Z. Y. Yu, X. Q. Cao and T. Sun, *Chem. Eng. J.*, **171**, 703 (2011).
12. S. Huijia, Z. Ying, L. Jia and T. Tianwei, *Process Biochem.*, **41**, 1422 (2006).
13. The Council of the European Communities, Directive 76/464/EEC on pollution caused by certain dangerous substances discharged into the aquatic environment of the community, *Off. J. Eur. Commun.* (1976) No. L 129/23.
14. D. R. Petrell, B. Ansari, P. Doig, J. Lam, H. Wong and L. Xu, *Aquat. Des. Rehabil.*, **1**, 75 (2002).
15. G. Basak, D. Charumathi and N. Das, *Int. J. Eng. Sci. Technol.*, **3**, 6321 (2011).
16. I. Langmuir, *J. Am. Chem. Soc.*, **38**, 2221 (1916).
17. H. M. F. Freundlich, *J. Phys. Chem.*, **57**, 385 (1906).
18. T. Fan, Y. Liu, B. Feng, G. Zeng, C. Yang, M. Zhou, H. Zhou, Z. Tan and X. Wang. *J. Hazard. Mater.*, **160**, 655 (2008).
19. S. Lagergren, *K. Sven. Vetenskapsakad. Handl.*, **24**, 1 (1898).
20. Y. S. Ho and G. McKay, *Chem. Eng. J.*, **70**, 115 (1978).
21. D. Das, G. Basak, Lakshmi. V and N. Das, *Biochem. Eng. J.*, **64**, 30 (2012).
22. V. K. Gupta, M. Gupta and S. Sharma, *Water Res.*, **35**, 1125 (2001).
23. A. J. Kora, R. Manjusha and J. Arunachalam, *Mater. Sci. Eng. C.*, **29**, 2104 (2009).
24. L. Jin and R. Bai, *Langmuir*, **18**, 9765 (2002).
25. B. D. Cullity, Elements of X-Ray Diffraction, Addison-Wesley, Reading, MA, USA, 3rd Ed. (1967).
26. B. Volesky, *Hydrometallurgy*, **59**, 203 (2001).
27. K. Fytianos, E. Voudrias and E. Kokkalis, *Chemosphere*, **40**, 3 (2000).
28. I. Tan, A. L. Ahmad and B. Hameed, *J. Hazard. Mater.*, **154**, 337 (2008).
29. M. M. Dubinin, *Chem. Rev.*, **60**, 235 (1960).
30. S. M. Hasany and M. H. Chaudhary, *Appl. Rad. Isot.*, **47**, 467 (1996).
31. Y. S. Ho and A. E. Ofomaja, *Biochem. Eng.*, **30**, 117 (2006).
32. A. Kumar, S. Kumar and D. V. Gupta, *J. Hazard. Mater.*, **147**, 155 (2007).
33. G. E. Boyd, A. W. Adamson and L. S. Myers, *J. Am. Chem. Soc.*, **69**, 2836 (1947).
34. D. Mohan and K. P. Singh, *Water Res.*, **36**, 2304 (2006).
35. A. M. E. I.- Kamash, A. A. Zaki and M. Abed-E.I- Geleel, *J. Hazard. Mater.*, **127**, 211 (2005).